Asian Research Journal of Mathematics

16(7): 34-58, 2020; Article no.ARJOM.56956
ISSN: 2456-477X

Numerical Analysis of the Flow of a Casson Fluid in Magnetic Field over an Inclined Nonlinearly Stretching Surface with Velocity Slip in a Forchheimer Porous Medium

Bhim Sen Kala[1*], Madan Singh Rawat[2] and Ajay Kumar[2]

[1]Doon University, Dehradun - 248001, Uttarakhand, India.
[2]HNB Garhwal University, Srinagar, Garhwal - 246744, Uttarakhand, India.

Authors' contributions

This work was carried out in collaboration among all authors. Author BSK designed the study, performed the statistical analysis, wrote the protocol and wrote the first draft of the manuscript. Authors MSR and AK managed the analyses of the study and the literature searches. All authors read and approved the final manuscript.

Article Information

DOI: 10.9734/ARJOM/2020/v16i730201
Editor(s):
(1) Prof. Megan M. Khoshyaran, ETC, Research Unit, France.
Reviewers:
(1) Charles Chinwuba Ike, Enugu State University of Science and Technology, Nigeria.
(2) Fateh Mebarek-Oudina, University of Skikda, Algeria.
Complete Peer review History: http://www.sdiarticle4.com/review-history/56956

Original Research Article

Received: 10 March 2020
Accepted: 15 May 2020
Published: 30 May 2020

Abstract

In this work, we have studied a magnetohydrodynamic, Casson fluid flow with velocity slip over an inclined nonlinearly stretching surface in Non-Darcy porous medium, numerically. In the mathematical model, we have transformed the momentum equation, energy equation and mass concentration equations to non-dimensional ordinary differential equations using similarity variables. We have solved the equations numerically by bvp4c using MATLAB for the numerical computation, and took $\eta_\infty = 12$ and axes so that figures are clearly visible. We have discussed and analysed the magnitude of the velocity, temperature, concentration, Local Skin friction, Local Nusselt number and Local Sherwood number using their representative parameters and the effects of these parameters on the respective boundary layer regions using graphs, figures and tables.

Keywords: Magnetic; Darcy; velocity slip; inclination parameter; Casson fluid; Forchheimer parameter; power index parameter.

Mathematics Subject Classification: 35A35, 35A99, 35G30.

**Corresponding author: E-mail: bhimskala@gmail.com;*

Nomenclatures

x , y *Cartesian coordinates[m]*
u *x-component of velocity [m/s]*
υ *y-component of velocity [m/s]*
B *magnetic field,*
B_0 *magnetic constant*
K_d *permeability parameter[m^2]*
Fs *Forchheimer parameter,*
ρ *fluid density [kg m^{-3}]*
ν *fluid kinematic viscosity [m^2 s^{-1}]*
μ *fluid dynamic viscosity [kg m^{-1} s^{-1}]‘*
μ_B *plastic dynamic viscosity fluid*
p_y *yield stress of fluid*
e_{ij} (i, j) *-th component of deformation rate*
π *product of deformation rate*
β_T *thermal expansion coefficient*
β_C *mass expansion coefficient*
K *solute’s chemical reaction rate*
g *gravity- acceleration*
α_T *thermal diffusivity of the fluid*
C_p *specific heat at constant pressure*
k *thermal conductivity of the fluid*
D *mass diffusion coefficient*
η *similarity variable,*
ψ *stream function [m^2 s^{-1}]*
f *non- dimensional stream function*
S *suction(blowing) parameter*
β *Casson fluid parameter,*
n *stretching power index parameter.*
α *inclination parameter*
M *non- dimensional Magnetic parameter*
K_p *non- dimensional Permeability parameter*
C_b *non- dimensional Forchheimer coefficient* Gr *Grashof number,*
Gc *solutal Grashof number,*
γ^* *buoyancy parameter,*
γ *solutal buoyancy parameter,*
K_c *chemical reaction parameter*
u_w *surface stretching speed,*
u_S *velocity slip*
. υ_w *wall mass transfer velocity*
Vs *Velocity slip parameter*
n *stretching surface power index parameter.*
$T(x)$ *temperature at the surface*
T_w *initial temperature of the surface*
T_0 *proportionality constant*
$\frac{\partial T}{\partial y}$ *temperature gradient term*
$C(x)$ *concentration at the surface*
C_w *initial concentration of the surface*
C_0 *proportionality constant*
$\frac{\partial C}{\partial y}$ *concentration gradient term*
T_∞ *ambient temperature*
C_∞ *ambient concentration*
C_f *local skin-friction*
Re_f *Reynold number.*
τ_w *Shearing stress*
Nu_x *local Nusselt number*
Sh_x *local Sherwood number*

1 Introduction

From the twentieth century we study boundary layer region in the engineering applications in industries like in metallurgy, metal processing and in chemical engineering, drawing of polymer sheets. Fluid may be Newtonian or non-Newtonian. Water is the example of Newtonian fluid where viscous force (stress) at the boundary of the surface is linearly proportional to the velocity gradient of the fluid. Honey, milk, fruit juice,

shampoos, sanitizer, paint, mud, blood, and other body fluids glues vegetable oil are examples of non-Newtonian fluid and their viscous force at the boundary surface are not linearly proportional to the velocity gradient. Casson fluid is one such example of non-Newtonian fluids. We consider fluid flow due to stretching of the surface.

Crane [1] started the study of the boundary layer region of the Newtonian fluid which being viscous and incompressible, flow over a linearly stretching surface. He considered the case of stretching velocity proportional to distance from the slit; plastic film manufacturing is its one example. The researchers took interest to study its extension to non Newtonian fluid and nonlinear stretching surfaces.

Rajagopal [2] analysed the viscous incompressible fluid flow in boundary layer region on moving (stretching) sheet. Ishak et al. [3] studied the boundary layer of laminar magneto-hydrodynamic viscous and incompressible fluid, with two dimentional flow over a moving wedge (FALKNER-SKAN boundary layer problem) with suction and injection.

Siddappa, B. and Abel Subhas [4] analysed the flow of visco-elastic fluid over the boundary layer region past a stretching plate. Andersson [5] studied the boundary layer region of magneto hydrodynamic non-newtonian fluid flow over a stretching surface. Dandapat et al. [6] studied the stable property of the viscoelastic fluid flow over a stretching sheet, in transverse magnetic field to the stretching surface.

Fang [7] analysed the solution of the extension of original Blasius boundary layer problem by solving that by variable transformation method. Mamaloukas et al. [8] discussed the exact solution of flow of visco-elastic fluid of second grade over a stretching surface, in two dimension using free-parameter method and separation of variable method.

Khidir Ahmed [9] applied iterative methods: Successive linearization method and spectral homotopy perturbation method, to solve the magnetohydrodynamic Falker-Skan nonlinear boundary layer problem. Bataller [10] analysed the boundary layer region of the electrically non conducting, viscous and incompressible fluid flow under two situations: over a moving plane in a fluid at rest (Sakiadis flow) and with uniform flow over a flat-plane at rest (Blasius flow).

Motsa, et al. [11] studied the boundary layer of the magnetohydrodynamic (MHD) upper-convected Maxwell (UCM) fluid flow on a porous stretching sheet. Motsa et al. [12] analysed the boundary layer region of the magneto-hydrodynamic viscous incompressible fluid flow over a nonlinearly stretching surface in the presence of transverse magnetic field. Rosca [13] analysed the boundary layer region of the MHD, viscous, incompressible, electrically conducting fluid flow over a shrinking permeable sheet. Nadeem et al. [14] studied the magnetohydrodynamic (MHD) Williamson fluid flow in the boundary layer region over a stretching surface.

Mukhopadhyay [15] analysed the MHD viscous incompressible fluid flow over a stretching cylinder in symmetric boundary layer about the axis of the cylinder under partial slip condition. Akbar et al. [16] investigated boundary layer of the MHD Carreau fluid flow over a permeable shrinking sheet. Nadeem S, et al. [17] investigated the MHD flow of a Casson fluid in the boundary layer region over an exponentially shrinking surface. Biswas et al. [18] analysed the unsteady magnetohydrodynamic Casson fluid flow along a vertical plate with chemical reaction and radiation effects.

Ahmmed et al. [19] discussed the unsteady magnetohydrodynamic nanofluid flow over an exponentially accelerated and inclined plate, in a porous medium with variable thermal conductivity and free convection, and radiation. Biswas et al. [20] analysed the boundary layer region for the flow along vertical plate of unsteady magneto hydrodynamic casson nanofluid with the Hall current and chemical reaction effects. Noor et al. [21] studied the MHD visco-elastic fluid of second grade with mixed convection, hall-current and thermophoresis effects over a stretching surface.

Sharada et al. [22] studied the boundary layer of magnetohydrodynamic Casson fluid flow over an exponentially stretching sheet with mixed convection, thermal radiation, dufour, soret and chemical reaction effects on it. Mukhopadhyay et al. [23] analysed the effect of transpiration and heat transfer on the boundary layer region of the Casson fluid flow over a linearly stretching sheet.

Jawad Raza, et al. [24] analysed boundary layer region for the nano Williamson fluid flow along a stretching surface having transverse magnetic field to the surface and with multiple slip. Jawad Raza, et al. [25] studied the boundary layer region for MHD non-Newtonian nanofluid flow along a nonlinear permeable stretching sheet with multiple slip effects. Mebarek Oudina [26] studied the Titania nanofluids (of different base fluids) flow in cylindrical annulus in the presence of heat source and heat convection.

Mebarek Oudina et al. [27] studied to the boundary layers of the nanofluid flow due to radially stretching disk in the presence of transverse magnetic field to the surface of the disk, coriolis force, heat source. Marzougui, et al. [28] studied the magnetohydrodynamic copper–water nanofluid flow in a cavity with chamfers for its entropy. J. Raza, et al. [29] investigated the boundary layer region for MHD non-newtonian molybdenum disulfide nanofluid flow in a converging or diverging channel and in the presence of radiation.

Kala [30-32] studied the boundary layer region of MHD flow of a Casson fluid over a non-linearly stretching sheet with partial slip in a non-Darcy porous medium and discussed the effects of Grashof number, modified Grashof number, chemical reaction, suction, slip and inclination parameters.

In this work we will numerically analysis the flow of Casson fluid under the influence of magnetic field applied in the transverse direction to the flow of the fluid and fluid flows through the non-Darcy porous medium, with velocity slip, the surface over which fluid flows, is non linear and inclined at some angle to the vertical. And the flow of the fluid is due to the stretching of the surface. The analysis of the effects of the magnitude of the velocity, temperature, concentration, Local Skin friction, Local Nusselt number and Local Sherwood number using their representative parameters on the respective boundary layer regions is done.

2 Mathematical Modelling

We consider two-dimensional, steady, laminar flow in boundary layer region of viscous, incompressible, and electrically conducting Casson fluid, along a nonlinearly stretching surface, inclined at an acute angle (α) to the vertical, in a saturated homogeneous Forchheimer porous medium.

In the study we consider cartesian coordinates: The stretching surface as x-axis and normal to it as the y-axis. We assume that during stretching, position of the origin remains unchanged; and stretching velocity at a point of the surface is non-linearly proportional to its distance from the origin and magnetic field of uniform strength B is normal to stretching surface.

Again we assume that fluid does not change its phase. In flow conditions we assumed that flow is in Forchheimer porous medium. It represents: the flow is with high velocity. And so the Forchheimer drag force is a resistance due to porous medium and is proportional to the square of fluid velocity. And we assume that it also includes resistance due to slow velocity of the fluid. Due to slow velocity there is a drag which is called Darcian drag force and it is linearly proportional to the velocity. Examples of high velocity occur in chemical engineering. In the model viscous drag, called Brinkman drag force, comes into existence at the surface of the sheet in the boundary layer region.

Again we assume that induced magnetic field, electric field due to charge particles in the fluid, and external electric field are negligible. And so Hall Effect and joule heating effect are negligible.

We assume that the thermal conductivity and viscosity of the fluid are constant. The temperature of the fluid and fluid mass concentration at the stretching surface are greater than their values in the free stream.

On considering theses assumptions, the rheological equation for the casson fluid are given as follows [22,23]

$$\tau_{ij} = 2\, e_{ij}\left(\mu_B + \frac{p_y}{\sqrt{2\pi}}\right) \quad if \quad \pi > \pi_c$$

$$\tau_{ij} = 2\, e_{ij}\left(\mu_B + \frac{p_y}{\sqrt{2\pi_c}}\right) \quad if \quad \pi < \pi_c$$

Where μ is the dynamic viscosity of the casson fluid, μ_B the plastic dynamic viscosity of the casson fluid, p_y the yield stress, of the casson fluid. π is the product of the deformation rate of casson fluid element with itself: $\pi = e_{ij}\, e_{ij}$ and e_{ij} is the (i, j) -th deformation rate. π_c is critical value of the product for the casson model.

Fig. 1 represents the boundary layer flow presentation and the coordinate system.

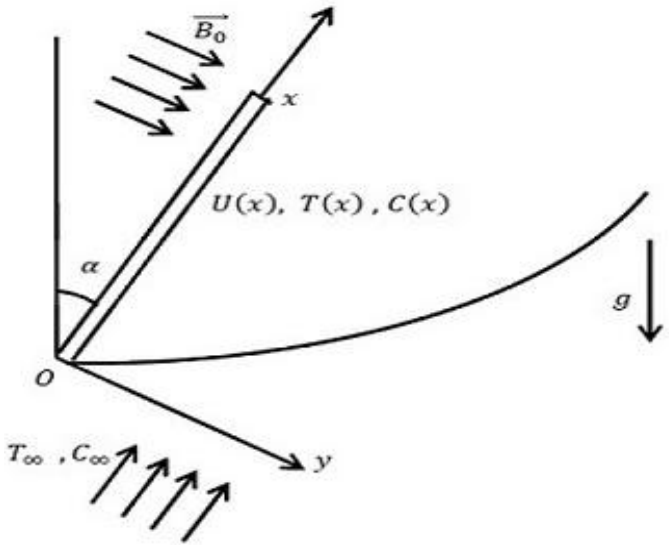

Fig. 1. The boundary layer flow presentation and the coordinate system for stretching surface

Under the above assumptions, the equations for momentum, energy and mass concentration to represent their flow in their respective boundary layer regions are given as follows:

The continuity equation

$$\frac{\partial u}{\partial x} + \frac{\partial v}{\partial y} = 0 \tag{1}$$

The Momentum: Equation

$$u\frac{\partial u}{\partial x} + v\frac{\partial u}{\partial y} = \left(1 + \frac{1}{\beta}\right)\frac{\partial^2 u}{\partial y^2} \pm g\begin{pmatrix}\beta_T (T - T_\infty)\\ +\beta_C (C - C_\infty)\end{pmatrix}\cos\alpha - \frac{\sigma B_0^2}{\rho_f}u - \frac{v}{K_d}u - \frac{C_b}{\sqrt{K_d}}u^2 \tag{2}$$

The Energy: Equation

$$u\frac{\partial T}{\partial x}+v\frac{\partial T}{\partial y}=\alpha\frac{\partial^2 T}{\partial y^2} \tag{3}$$

The Mass concentration Equation:

$$u\frac{\partial C}{\partial x}+v\frac{\partial C}{\partial y}=D\frac{\partial^2 C}{\partial y^2}-K_C(C-C_\infty) \tag{4}$$

here, the $\pm$ refers to assisting and opposing flow (assisting flow for positive sign and opposing flow for negative sign), x coordinate along the stretching sheet and y coordinate normal to the stretching sheet respectively, u is the x - component of velocity and v is y-component of velocity, K_d is the porous medium's permeability, B the magnetic field, C_b the Forchheimer coefficient, α the angle of inclination ofthe surface with the vertical of the surface, β the parameter of Casson fluid, μ, υ and ρ are dynamic viscosity ,kinematic viscosity and density of the fluid respectively. K , β_C and β_T are, the chemical reaction rate, the mass expansion coefficient and the thermal expansion coefficient of the solute, respectively. g is gravitational acceleration. $\alpha_T = k/(\rho C_p)$ is the thermal diffusion coefficient of the fluid , C_p the specific heat at constant pressure, k the thermal conductivity, and D mass diffusion coefficient of the fluid.

The magnetic field strength is assumed to be $B(x)=B_0\ x^{(n-1)/2}$ where B_0 is constant.

It is assumed that the sheet moves following velocity power law, and varying nonlinearly with respect to position coordinates with some power as index, in the boundary layer field, and follows following boundary conditions for equations (1) to (4):

$$\left.\begin{array}{c}\text{At } y=0,-\infty<x<\infty:\\ u=U(x)=u_w+u_S=cx^n+N\mu\frac{\partial u}{\partial y},\\ v=v_w=-V(x)\\ T(x)=T_w+T_0\frac{\partial T}{\partial y}, C(x)=C_w+C_0\frac{\partial C}{\partial y}\\ \text{As } y\to\infty, u\to 0, T\to T_\infty, C\to C_\infty\end{array}\right]. \tag{5}$$

where u_w is the velocity of the sheet with $u_w = c\,x^n$, c being a constant depending upon the velocity of the stretching surface, u_S is the slip velocity, proportional to the local shear stress given as follows: $u_S = N\mu\ \dfrac{\partial u}{\partial y} = N\left(\mu_B + p_y/\sqrt{2\pi}\right)\dfrac{\partial u}{\partial y}$, N ($m^2\ s\ kg^{-1}$) being the slip constant. $\mu = \left(\mu_B + p_y/\sqrt{2\pi}\right)$ the dynamic viscosity, $\beta = \mu_B\sqrt{2\pi}/p_y$ the Casson fluid parameter. v_w the velocity of mass transfer at the surface with $v_w > 0$ representing mass suction and $v_w < 0$ representing mass injection. n is the index parameter of the stretching surface, $n>0$ representing accelerated sheet and $n<0$ representing decelerated sheet.

$T(x)$ is temperature at a distance x along the surface from the origin, T_W initial temperature at the surface , T_0 is proportionality constant with $\frac{\partial T}{\partial y}$ the temperature gradient. $C(x)$ is concentration at a distance x along the surface from the origin, C_W is initial concentration at the surface, C_0 is proportionality constant with $\frac{\partial C}{\partial y}$ the concentration gradient. T_∞ and C_∞ are temperature and concentration faraway from their respective boundary layers.

Dimensional analysis: We define

$$\left.\begin{gathered} \eta = \sqrt{\frac{c\,(n+1)}{2\upsilon}}\, x^{\frac{(n-1)}{2}} y\,, \psi = \sqrt{\frac{2\,c\,\upsilon}{(n+1)}}\, x^{\frac{(n+1)}{2}} f(\eta), \\ u = \frac{\partial \psi}{\partial y}\,, v = -\frac{\partial \psi}{\partial x}, \\ u = c\, x^n f'(n)\,, v = -\sqrt{\frac{c\,\upsilon\,(n+1)}{2}}\, x^{\frac{(n-1)}{2}} \left(f(\eta) + \frac{(n-1)}{(n+1)}\, \eta\, f'(\eta) \right) \\ \theta(\eta) = \frac{(T - T_\infty)}{(T_w - T_\infty)}\,, \phi(\eta) = \frac{(C - C_\infty)}{(C_w - C_\infty)} \end{gathered}\right\}. \tag{6}$$

where η is similarity variable, ψ stream function, f non-dimensional stream function, u , x -component of velocity, υ , y- component of velocity.

Using above equations (6), in equations (1) to (4) we get following forms of the equations.

$$\left(1 + \tfrac{1}{\beta}\right) f''' + f\, f'' + \tfrac{2n}{(n+1)}\, f'^2 + \tfrac{2}{(n+1)}\, (\gamma^*\, \theta + \gamma\, \phi) \cos\alpha - \tfrac{2}{(n+1)} \left(\left(M + \tfrac{1}{K_p} \right) f' + Fs\, (f')^2 \right) = 0, \tag{7}$$

$$\tfrac{1}{Pr}\, \theta'' + f\, \theta' = 0, \tag{8}$$

$$\tfrac{1}{Sc}\, \phi'' + f\, \phi' - \tfrac{2}{(n+1)} K_c \phi = 0, \tag{9}$$

And corresponding boundary conditions (5) take the following forms:

$$\left.\begin{gathered} f(0) = S, f'(0) = 1 + Vs\, f''(0), \theta(0) = 1 + \lambda t\, \theta'(0) \\ \phi(0) = 1 + \lambda c\, \phi'(0) \\ f'(\eta) \to 0, \theta(\eta) \to 0, \phi(\eta) \to 0, \text{as } \eta \to \infty \\ \text{Where } \lambda t = T_0 \sqrt{\frac{c\,(n+1)}{2\upsilon}}\, x^{\frac{(n-1)}{2}}, \lambda c = C_0 \sqrt{\frac{c\,(n+1)}{2\upsilon}}\, x^{\frac{(n-1)}{2}} \end{gathered}\right\}. \tag{10}$$

Here differentiation with respect to η is represented by prime.

In equations (7) to (10), we define parameters as follows:

$M = \dfrac{\sigma B_0^2}{c\,\rho_f}$ Magnetic parameter, $K_p = \dfrac{cK_d\, x^{(n-1)}}{\upsilon}$ Permeability parameter, $Fs = \frac{c_b x}{\sqrt{K_d}}$ Forchhiemer parameter, $Gr = \dfrac{g\,\beta_T (T_w - T_\infty)\, x^2}{\upsilon^2}$ Grashof number, $Gc = \dfrac{g\,\beta_C (C_w - C_\infty)\, x^2}{\upsilon^2}$ solutal Grashof

number, $\gamma^* = \frac{Gr}{\mathrm{Re}^2}$ buoyancy parameter, $\gamma = \frac{Gc}{\mathrm{Re}^2}$ solutal buoyancy parameter, $\mathrm{Re}_x = \frac{u_w x}{\upsilon}$ Reynolds number, $u_w = c\,x^n$ fluid velocity along the the surface at distance x from the origin, $Sc = \frac{\upsilon}{D}$ Schmidt number, $\mathrm{Pr} = \frac{\upsilon}{\alpha_T}$ Prandtl number, $K_c = K^{-1}x^{1-n}$ reaction rate parameter, $K_c > 0$ represents destructive chemical reaction, $K_c = 0$ represents no reaction and $K_c < 0$, represents constructive chemical reaction. $S = -v_w\sqrt{\frac{2}{\upsilon c(n+1)}}\,x^{\frac{(1-n)}{2}}$ suction/injection parameter, $S > 0$ represents suction and $S < 0$ represents injection or blowing ($v_w < 0$ represents mass suction and $v_w > 0$ represents mass injection). $Vs = N\mu\sqrt{\frac{c(n+1)}{2\,\upsilon}}\,x^{\frac{(n-1)}{2}}$ parameter of slip velocity. λt slip parameter for temperature λc slip parameter for concentration.

The local Skin-friction coefficient Cf_x the local Nusselt number Nu_x, the local Sherwood number Sh_x and Reynold number (Re_x) , are important in engineering designs and are given as follows:

The local Skin-friction coefficient is $Cf_x = \frac{\tau_w}{\rho_f u_w^2}$.

The Shearing Stress is $\tau_w = \mu_B \left(1 + \frac{1}{\beta}\right)\left(\frac{\partial u}{\partial y}\right)_{y=0}$,

$$\tau_w = \mu \left(\frac{\partial u}{\partial y}\right)_{y=0} = \left(\mu_B + \frac{p_y}{\sqrt{2\pi}}\right)\left(\frac{\partial u}{\partial y}\right)_{y=0}.$$

The local Reynold number is $Re_x = \frac{u_w x}{v}$.

$$Cf_x = \frac{\left(\mu_B + \frac{p_y}{\sqrt{2\pi}}\right)\left(\frac{\partial u}{\partial y}\right)_{y=0}}{\rho_f u_w^2} = \frac{1}{\sqrt{Re_x}}\sqrt{\frac{n+1}{2}}\left(1 + \frac{1}{\beta}\right) f''(0)\,. \tag{11}$$

Local Nusselt number

$$Nu_x = \frac{-x\left(\frac{\partial T}{\partial y}\right)_{y=0}}{T_w - T_\infty} = -\frac{1}{\sqrt{Re_x}}\sqrt{\frac{n+1}{2}}\,\theta'(0). \tag{12}$$

Local Sherwood number:

$$\mathrm{Sh_x} = \frac{-x\left(\frac{\partial C}{\partial y}\right)_{y=0}}{C_w - C_\infty} = -\frac{1}{\sqrt{Re_x}}\sqrt{\frac{n+1}{2}}\,\phi'(0). \tag{13}$$

3 Method of Numerical Solution

We assign different values to the parameters: Casson (β), velocity slip (Vs), inclination (α), Stretching index (n), the Magnetic (M), the Permiability porosity (Kp), and the Forchhemier (Fs), and obtain the solution of the model using bvp4c, numerically in MATLAB. We put $\eta_\infty = 12$ axis so that figures are explicitly visible.

4 Results and Analysis

We consider the results of Andersson [4], Mahdy [16] and Ahmed [17] for the skin friction coefficient $f''(0)$ for comparison with our results. We use the parameter values: M =1; Kp =1; Fs =1; α =0.2; β =0.5; n =1; Vs =0.2; γ^* =0.5; γ = 0.5; Pr =1; Sc =1; Kc =0.5; S =0.2; λt =1; λc =1; and skin friction f0(3)=0.2; nusselt value f0(5)=0.2; sherwood value f0(7)=0.2 in our our equations to get the work of these authors. The skin friction values $f''(0)$ of our result and of results of the authors are tabulated in Table 1.

Table 1. Table for the skin friction coefficient $f''(0)$ calculated presently in this work and in the works of Andersson [4], Mahdy [16] and Ahmed[17] for the parameters Vs=[0.0;0.1;0.5;1.0], β =inf, M=0, Kp=inf, Fs=0 , n=1, γ^* =0.0, γ =0.0, α =0.0 , Pr=0, Sc=0, Kc =0.0, S=0.0, λt =0, λc =0, f0(3)=0.0, f0(5)=0.0, f0(7)=0.0 with $\eta_\infty = 12$

Vs	$f''(0)$ Andersson [4]	$f''(0)$ Mahdy [16]	$f''(0)$ Ahmed [17]	$f''(0)$ Present study [P]
0.0	-1.0000 [4]	-1.000000 [16]	-1.0000 [17]	-1.0000011136721379[P]
0.1	-0.8721 [4]	-0.8721091 [16]	-0.87208 [17]	-0.872083949541335[P]
0.5	-0.5912 [4]	-0.591199 [16]	-0.591195 [17]	-0.591197864801179[P]
1.0	-0.4302 [4]	-0.4302 001[16]	-0.430160 [17]	-0.430163666996962[P]

Table 1 shows the skin friction coefficient $f''(0)$ of this work match with works of Andersson [4], Mahdy [16] and Ahmed [17]. So our numerical method is justified.

We consider the following parameter values for Figs. 2 - 40 and Tables 3 - 20:

M =1; Kp =1; Fs =1; α =0.2; β =0.5; n =1; Vs =0.2; γ^* =0.5; γ = 0.5; Pr =1; Sc =1; Kc =0.5; S =0.2; λt =1; λc =1; f0(3)=0.2; f0(5)=0.2; and f0(7)=0.2;

Table 1. We consider following values of the parameters to draw the Figs. 2 to 40

	Fjg. 2to7	Fjg. 8to13	Fjg. 14to19	Fjg. 20to25	Fjg. 26to28	Fjg. 29to34	Fjg. 35to40
Vs	0.2	0.2	0.2	0.2	0.2	0.2	0.2, 1, 2.5, 3.5
n	1	1	1	1	1	0.5,1,2,3	1
β	0.5	0.5	0.5	0.5	0.5, 1.0, 2.5, 3.5	0.5	0.5
α	0.2	0.2	0.2	0.2, 1.0, 2.5, 3.5	0.2	0.2	0.2
Fs	1	1	0.2, 1.0, 2.5, 3.5	1	1	1	1
Kp	1	0.2, 1.0, 2.5, 3.5	1	1	1	1	1
M	0.2, 1.0, 2.5, 3.5	1	1	1	1	1	1

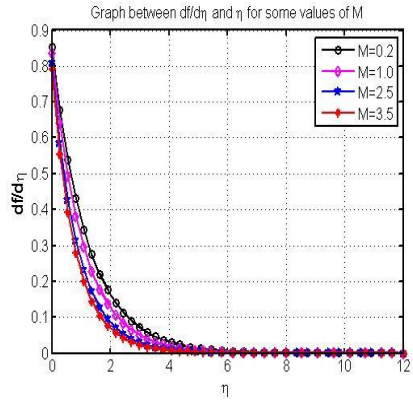

Fig. 2. Graph between $f'(\eta)$ and η for different values of M

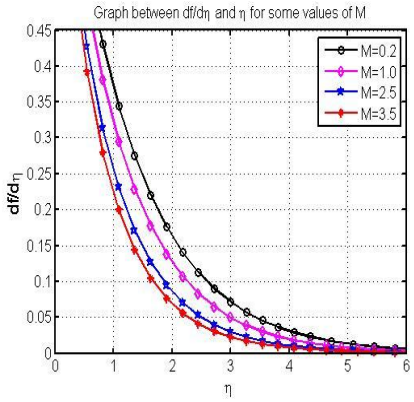

Fig. 3. Graph between $f'(\eta)$ and η for different values of M

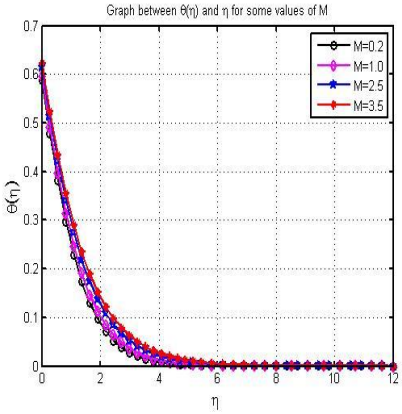

Fig. 4. Graph between $\theta(\eta)$ and η for different values of M

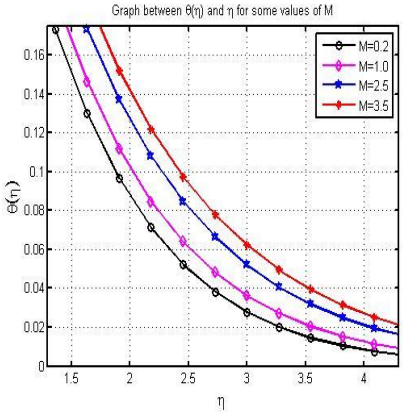

Fig. 5. Graph between $\theta(\eta)$ and η for different values of M

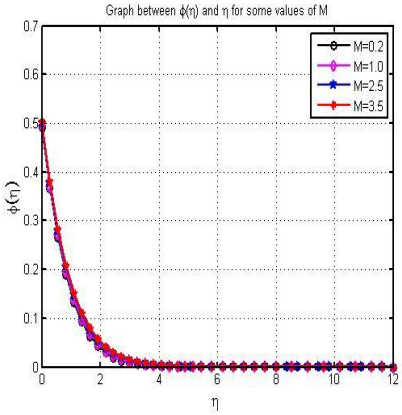

Fig. 6. Graph between $\phi(\eta)$ and η for different values of M

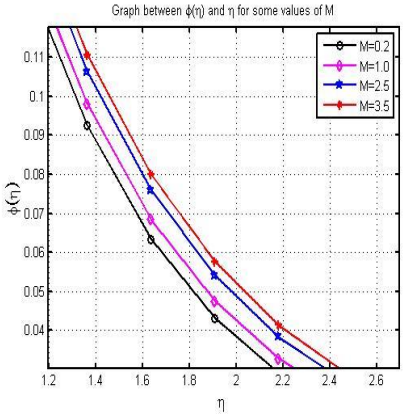

Fig. 7. Graph between $\phi(\eta)$ and η for different values of M

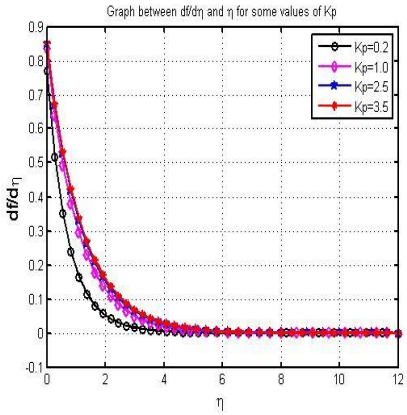

Fig. 8. Graph between $f'(\eta)$ and η for different values of Kp

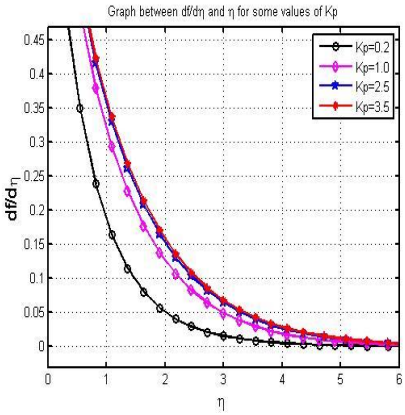

Fig. 9. Graph between $f'(\eta)$ and η for different values of Kp

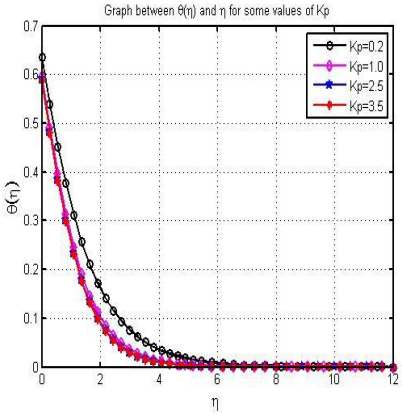

Fig. 10. Graph between $\theta(\eta)$ and η for different values of *Kp*

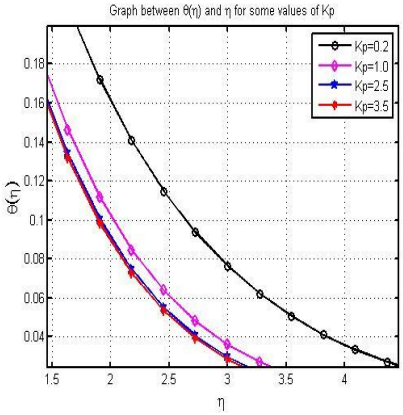

Fig. 11. Graph between $\theta(\eta)$ and η for different values of *Kp*

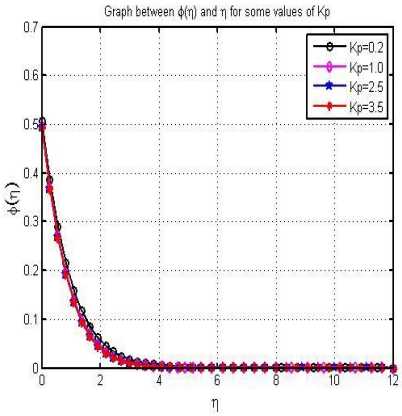

Fig. 12. Graph between $\phi(\eta)$ and η for different values of *Kp*

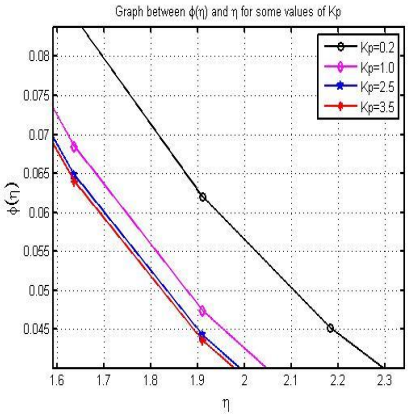

Fig. 13. Graph between $\phi(\eta)$ and η for different values of *Kp*

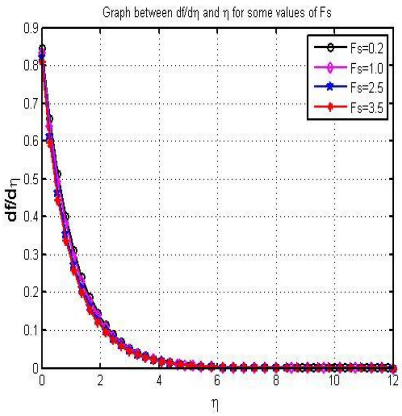

Fig. 14. Graph between $f'(\eta)$ and η for different values of *Fs*

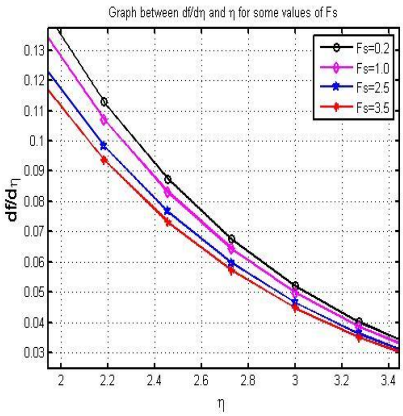

Fig. 15. Graph between $f'(\eta)$ and η for different values of *Fs*

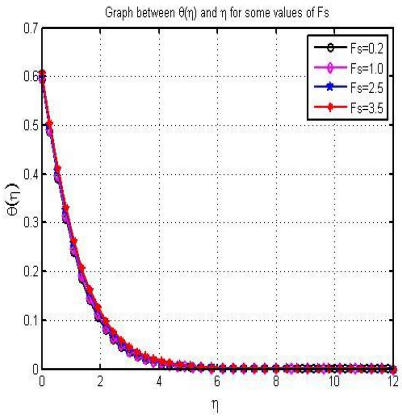

Fig. 16. Graph between $\theta(\eta)$ and η for different values of *Fs*

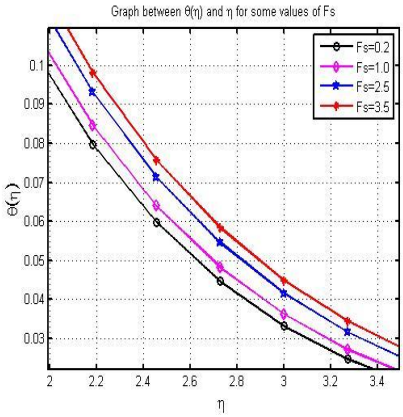

Fig. 17. Graph between $\theta(\eta)$ and η for different values of *Fs*

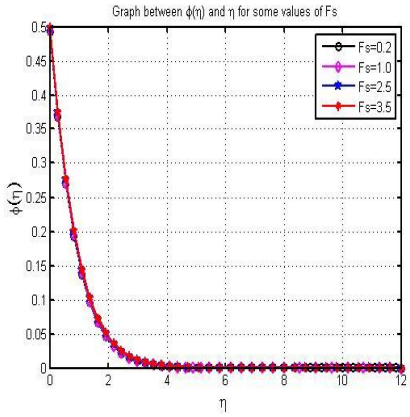

Fig. 18. Graph between $\phi(\eta)$ and η for different values of *Fs*

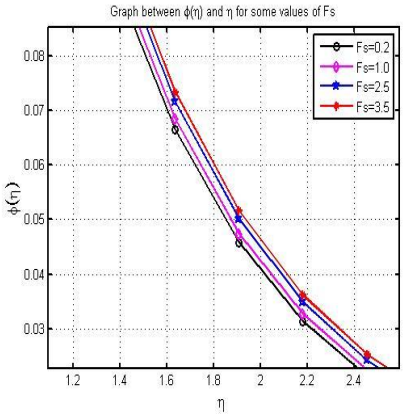

Fig. 19. Graph between $\phi(\eta)$ and η for different values of *Fs*

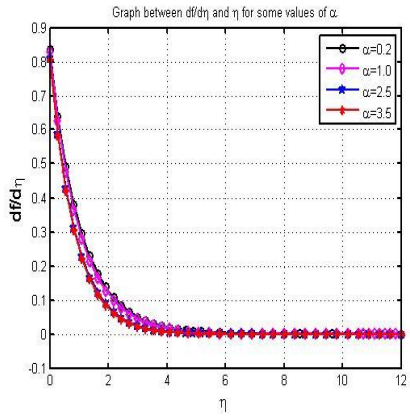

Fig. 20. Graph between $f'(\eta)$ and η for different values of α

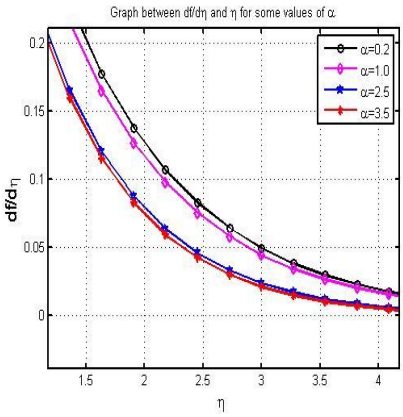

Fig. 21. Graph between $f'(\eta)$ and η for different values of α

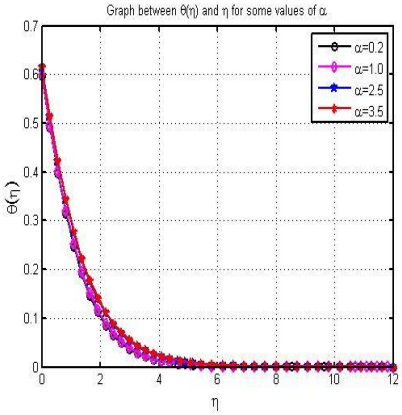

Fig. 22. Graph between $\theta(\eta)$ and η for different values of α

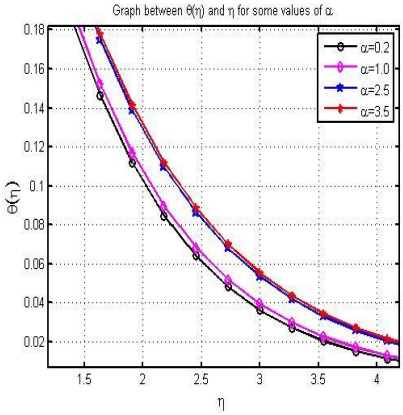

Fig. 23. Graph between $\theta(\eta)$ and η for different values of α

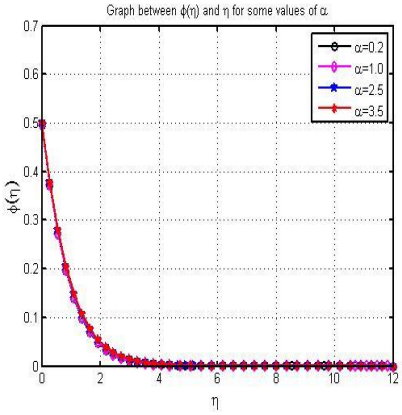

Fig. 24. Graph between $\phi(\eta)$ and η for different values of α

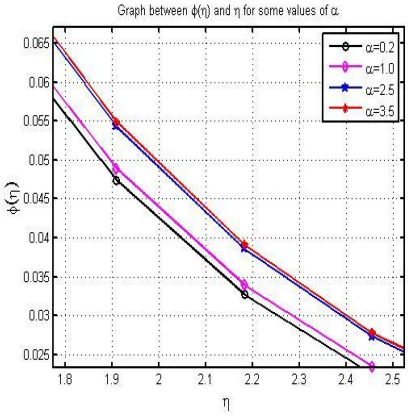

Fig. 25. Graph between $\phi(\eta)$ and η for different values of α

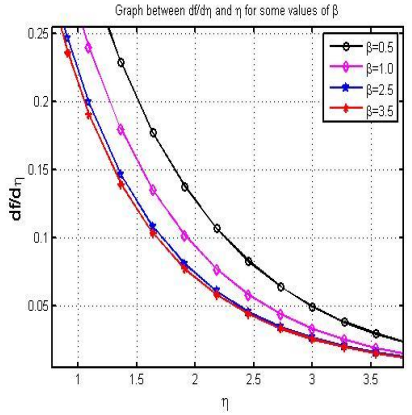

Fig. 26. Graph between $f'(\eta)$ and η for different values of β

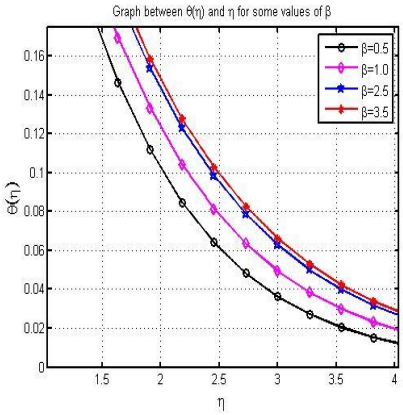

Fig. 27. Graph between $\theta(\eta)$ and η for different values of β

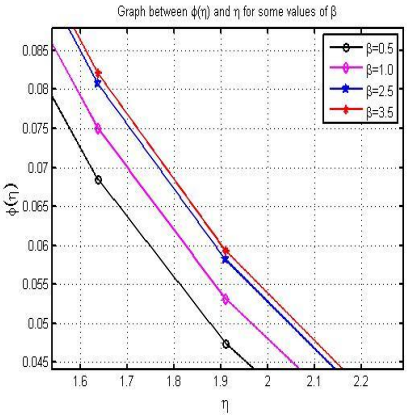

Fig. 28. Graph between $\phi(\eta)$ and η for different values of β

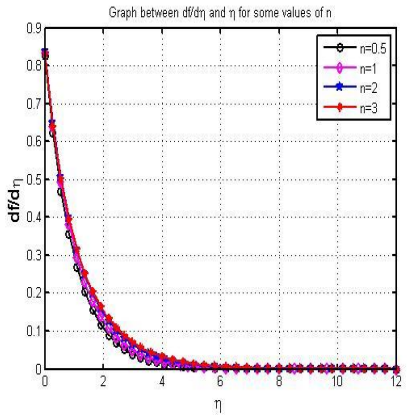

Fig. 29. Graph between $f'(\eta)$ and η for different values of n

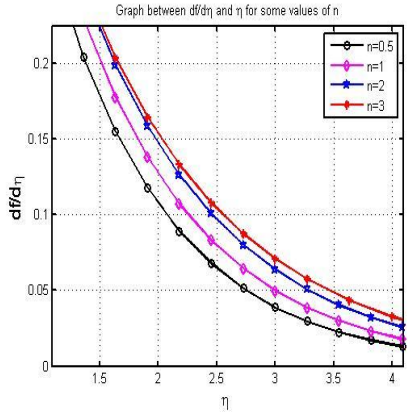

Fig. 30. Graph between $f'(\eta)$ and η for different values of n

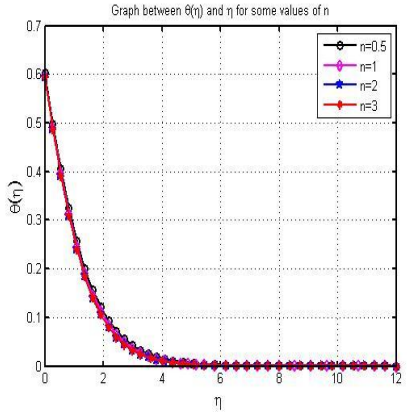

Fig. 31. Graph between $\theta(\eta)$ and η for different values of n

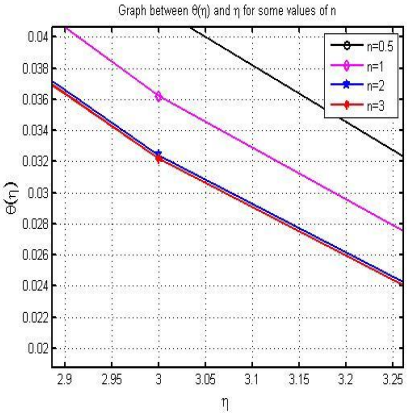

Fig. 32. Graph between $\theta(\eta)$ and η for different values of n

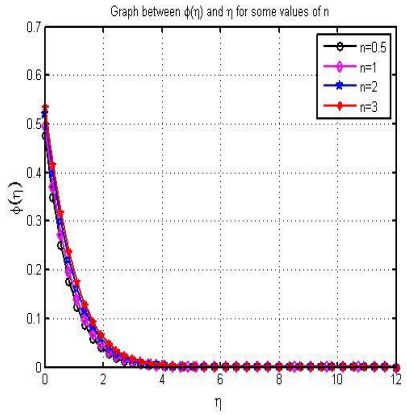

Fig. 33. Graph between $\phi(\eta)$ and η for different values of n

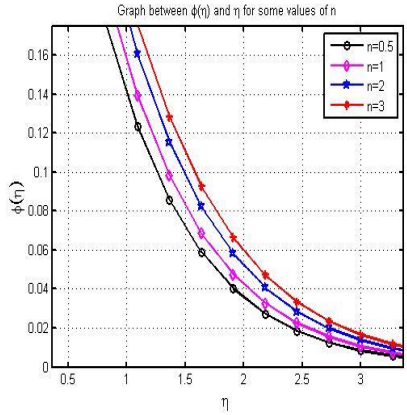

Fig. 34. Graph between $\phi(\eta)$ and η for different values of n

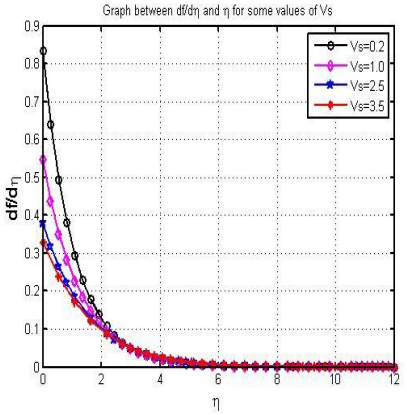

Fig. 35. Graph between $f'(\eta)$ and η for different values of Vs

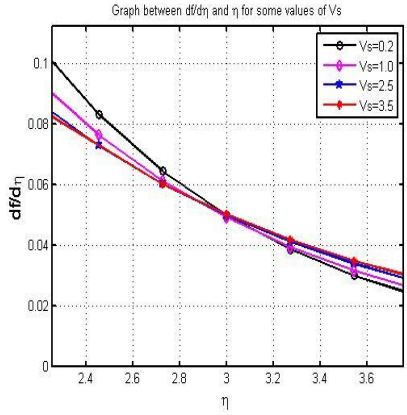

Fig. 36. Graph between $f'(\eta)$ and η for different values of Vs

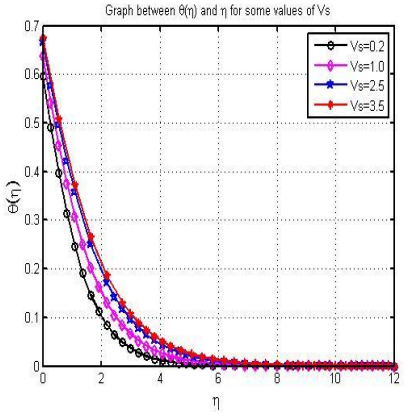

Fig. 37. Graph between $\theta(\eta)$ and η for different values of Vs

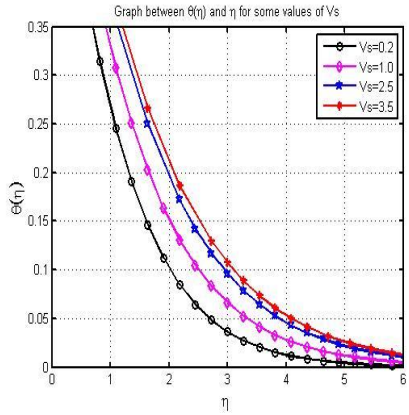

Fig. 38. Graph between $\theta(\eta)$ and η for different values of Vs

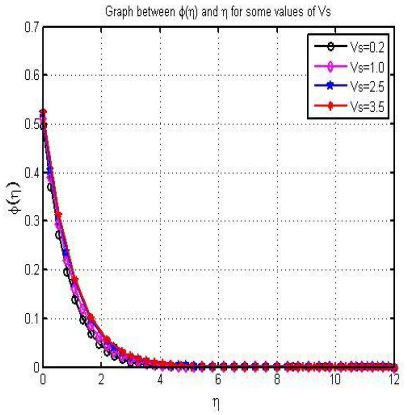

Fig. 39. Graph between $\phi(\eta)$ and η for different values of Vs

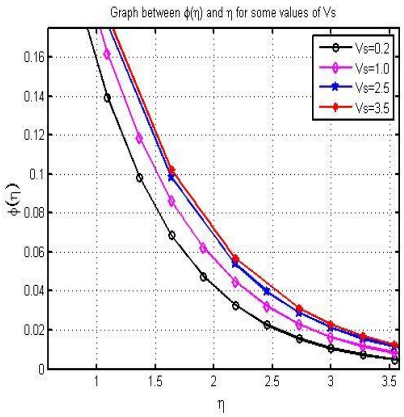

Fig. 40. Graph between $\phi(\eta)$ and η for different values of Vs

Fig. 2 is for $\mathbf{0} \leq \boldsymbol{\eta} \leq \mathbf{12}$. Fig. 3 is expansion of small part of Fig. 2 for $\mathbf{0} \leq \boldsymbol{\eta} \leq \mathbf{6}$. Figs. 2 or 3 shows thickness of velocity boundary layer and the absolute value of the velocity decrease with the increase in the value of the magnetic parameter *M*.

Fig. 4 is for $\mathbf{0} \leq \boldsymbol{\eta} \leq \mathbf{12}$. Fig. 5 is expansion of small part of Fig. 4 for $\mathbf{0} \leq \boldsymbol{\eta} \leq \mathbf{4}$. Figs. 4 and 5 shows thickness of thermal boundary layer and the absolute of the temperature increase and this increase speeds up with the increase in the value of the magnetic parameter *M*.

Fig. 6 is for $\mathbf{0} \leq \boldsymbol{\eta} \leq \mathbf{12}$. Fig. 6 is expansion of small part of Fig. 7 for $\mathbf{1.4} \leq \boldsymbol{\eta} \leq \mathbf{2.8}$. Figs. 6 and 7 shows thickness of concentration l boundary layer and the absolute of the concentration increase and this increase speeds up with the increase in the value of the magnetic parameter *M*.

Fig. 8 is for $\mathbf{0} \leq \boldsymbol{\eta} \leq \mathbf{12}$. Fig. 9 is expansion of small part of Fig. 8 for $\mathbf{1.5} \leq \boldsymbol{\eta} \leq \mathbf{5}$. Figs. 8 and 9 shows thickness of velocity boundary layer and the absolute value of the velocity increase and this increase slows down with the increase in the value of the porosity parameter *Kp*.

Fig. 10 is for $\mathbf{0} \leq \boldsymbol{\eta} \leq \mathbf{12}$. Fig. 11 is expansion of small part of Fig. 10 for $\mathbf{0} \leq \boldsymbol{\eta} \leq \mathbf{6}$. Figs. 10 and 11 shows thickness of thermal boundary layer and the absolute of the temperature decrease and also this decrease slows down with the increase in the value of the porosity parameter *Kp*.

Fig. 12 is for $\mathbf{0} \leq \boldsymbol{\eta} \leq \mathbf{12}$. Fig. 13 is expansion of small part of Fig. 12 for $\mathbf{2.4} \leq \boldsymbol{\eta} \leq \mathbf{3.2}$. Figs. 12 and 13 shows thickness of concentration l boundary layer and the absolute of the concentration decrease and this decrease slows down as the porosity parameter *Kp* increases.

Fig. 14 is for $\mathbf{0} \leq \boldsymbol{\eta} \leq \mathbf{12}$. Fig. 15 is expansion of small part of Fig. 14 for $\mathbf{1.6} \leq \boldsymbol{\eta} \leq \mathbf{3.0}$. Figs. 14 and 15 shows thickness of velocity boundary layer and the absolute value of the velocity decrease as the Forchheimer parameter *Fs* increases .and this decrease speeds up with the increase in the value of the Forchheimer parameter *Fs*.

Fig. 16 is for $\mathbf{0} \leq \boldsymbol{\eta} \leq \mathbf{12}$. Fig. 17 is expansion of small part of Fig. 16 for $\mathbf{2} \leq \boldsymbol{\eta} \leq \mathbf{3.6}$. Figs. 16 and 17 shows thickness of thermal boundary layer and the absolute of the temperature increase and this increase speeds up with the increase in the value of the Forchheimer parameter *Fs*.

Fig. 18 is for $\mathbf{0} \leq \boldsymbol{\eta} \leq \mathbf{12}$. Fig. 19 is part of Fig. 18 for $2 \leq \boldsymbol{\eta} \leq \mathbf{3.6}$. Figs. 18 and 19 shows thickness of concentration l boundary layer and the absolute of the concentration increase and this increase speeds up with the increase in the value of the Forchheimer parameter *Fs*.

Fig. 21 for $\mathbf{1.5} \leq \boldsymbol{\eta} \leq \mathbf{4.5}$ is expansion of small part of Fig. 20 for $\mathbf{0} \leq \boldsymbol{\eta} \leq \mathbf{12}$. Fig. 21 shows thickness of velocity boundary layer and the absolute value of the velocity decrease and this decrease speeds up with the increase in the value of the inclination parameter $\boldsymbol{\alpha}$.

Fig. 23 for $\mathbf{1.5} \leq \boldsymbol{\eta} \leq \mathbf{4.5}$ is expansion of small part of Fig. 22 for $\mathbf{0} \leq \boldsymbol{\eta} \leq \mathbf{12}$. Fig. 23 shows thickness of thermal boundary layer and the absolute of the temperature increase and this increase speeds up with the increase in the value of the inclination parameter $\boldsymbol{\alpha}$.

Fig. 25 for $\mathbf{1.2} \leq \boldsymbol{\eta} \leq \mathbf{2.6}$ is expansion of small part of Fig. 24 for $\mathbf{0} \leq \boldsymbol{\eta} \leq \mathbf{12}$. Fig. 25 shows thickness of concentration l boundary layer and the absolute of the concentration increase and this increase speeds up with the increase in the value of the inclination parameter $\boldsymbol{\alpha}$.

Fig. 26 for $\mathbf{0.75} \leq \boldsymbol{\eta} \leq \mathbf{3.75}$ is expansion of small part of Figure for $\mathbf{0} \leq \boldsymbol{\eta} \leq \mathbf{12}$. Fig. 26 shows thickness of velocity boundary layer and the absolute value of the velocity decrease and this decrease slows down with the increase in the value of the Casson parameter $\boldsymbol{\beta}$.

Fig. 27 for $\mathbf{1.0} \leq \boldsymbol{\eta} \leq \mathbf{4.0}$ is expansion of small part of Figure for $\mathbf{0} \leq \boldsymbol{\eta} \leq \mathbf{12}$. Figure shows thickness of thermal boundary layer and the absolute of the temperature increase and this increase slows down with the increase in the value of the Casson parameter $\boldsymbol{\beta}$.

Fig. 28 for $\mathbf{1.55} \leq \boldsymbol{\eta} \leq \mathbf{2.3}$ is expansion of small part of Figure for $\mathbf{0} \leq \boldsymbol{\eta} \leq \mathbf{12}$. Fig. 28 shows thickness of concentration l boundary layer and the absolute of the concentration increase and this increase slows down with the increase in the value of the Casson parameter $\boldsymbol{\beta}$.

Fig. 30 for $\mathbf{2} \leq \boldsymbol{\eta} \leq \mathbf{5.0}$ is expansion of small part of Fig. 29 for $\mathbf{0} \leq \boldsymbol{\eta} \leq \mathbf{12}$. Fig. 30 shows thickness of velocity boundary layer and the absolute value of the velocity increase and this increase slows down with the increase in the value of the stretching index parameter $\boldsymbol{n}$.

Fig. 32 for $\mathbf{2.9} \leq \boldsymbol{\eta} \leq \mathbf{3.25}$ is expansion of small part of Figure for $\mathbf{0} \leq \boldsymbol{\eta} \leq \mathbf{12}$. Fig. 32 (which is part of Fig. 31) shows thickness of thermal boundary layer and the absolute of the temperature decrease and this decrease slows down with the increase in the value of the stretching index parameter $\boldsymbol{n}$. Transition from n=2 to n=3 shows wavy nature of the temperature layer at or near the surface.

Fig. 34 for $\mathbf{0} \leq \boldsymbol{\eta} \leq \mathbf{3.5}$ is expansion of small part of Fig. 33 for $\mathbf{.0} \leq \boldsymbol{\eta} \leq \mathbf{12}$. Fig. 34 shows thickness of concentration l boundary layer and the absolute of the concentration increase and this increase slows down with the increase in the value of the velocity slip parameter.

Fig. 36 is expansion of small part of Fig. 35 for $\mathbf{0} \leq \boldsymbol{\eta} \leq \mathbf{12}$. Fig. 36 shows thickness of velocity boundary layer and the absolute value of the velocity decrease with the increase in the value of the velocity slip parameter.

Fig. 38 for $\mathbf{0.0} \leq \boldsymbol{\eta} \leq \mathbf{7}$ is expansion of small part of Fig. 37 for $\mathbf{.0} \leq \boldsymbol{\eta} \leq \mathbf{12}$. Fig. 38 shows thickness of thermal boundary layer and the absolute of the temperature increase with the increase in the value of the velocity slip parameter.

Fig. 40 for $\mathbf{1.5} \leq \boldsymbol{\eta} \leq \mathbf{3.2}$ is expansion of small part of Fig. 39 for $\mathbf{.0} \leq \boldsymbol{\eta} \leq \mathbf{12}$. Fig. 40 shows thickness of concentration l boundary layer and the absolute of the concentration increase and this increase slows down with the increase in the value of the velocity slip parameter.

Table 2. The local Skin friction $f''(0)$ for different values of β and M

$M \downarrow \backslash \beta \rightarrow$	$\beta = 0.50$ local Skin friction ,	$\beta = 1.0$ local Skin friction ,	$\beta = 2.5$ local Skin friction ,	$\beta = 3.5$ local Skin friction ,
0.2	-0.7335	-0.8516	-0.9654	-0.9939
1.0	-0.8252	-0.9579	-1.0859	-1.1180
2.5	-0.9658	-1.1195	-1.2673	-1.3043
3.5	-1.0443	-1.2087	-1.3664	-1.4057

Table 3 The local Nusselt Number $-\theta'(0)$ for different values of β and M

$M \downarrow \backslash \beta \rightarrow$	$-\theta'(0), \beta = 0.5$	$-\theta'(0), \beta = 1.0$	$-\theta'(0), \beta = 2.5$	$-\theta'(0), \beta = 3.5$
0.2	0.4133	0.4007	0.3891	0.3863
1.0	0.4028	0.3885	0.3754	0.3723
2.5	0.3863	0.3696	0.3547	0.3512
3.5	0.3770	0.3591	0.3435	0.3398

Table 4 The local Sherwood Number $-\phi'(0)$ for different values of β and M

$M \downarrow \backslash \beta \rightarrow$	$-\phi'(0), \beta = 0.5$	$-\phi'(0), \beta = 1.0$	$-\phi'(0), \beta = 2.5$	$-\phi'(0), \beta = 3.5$
0.2	0.5085	0.5042	0.5003	0.4994
1.0	0.5049	0.5002	0.4961	0.4952
2.5	0.4997	0.4946	0.4902	0.4892
3.5	0.4969	0.4917	0.4872	0.4862

Table 5. The local Skin friction $f''(0)$ for different values of β and Kp

$Kp \downarrow \backslash \beta \rightarrow$	$\beta = 0.50$ local Skin friction ,	$\beta = 1.0$ local Skin friction ,	$\beta = 2.5$ local Skin friction ,	$\beta = 3.5$ local Skin friction ,
0.2	-1.1462	-1.3236	-1.4929	-1.5350
1.0	-0.8252	-0.9579	-1.0859	-1.1180
2.5	-0.7578	-0.8799	-0.9976	-1.0271
3.5	-0.7440	-0.8639	-0.9794	-1.0083

Table 6. The local Nusselt Number $-\theta'(0)$ for different values of β and Kp

$Kp \downarrow \backslash \beta \rightarrow$	$-\theta'(0), \beta = 0.5$	$-\theta'(0), \beta = 1.0$	$-\theta'(0), \beta = 2.5$	$-\theta'(0), \beta = 3.5$
0.2	0.3647	0.3457	0.3294	0.3256
1.0	0.4028	0.3885	0.3754	0.3723
2.5	0.4105	0.3975	0.3855	0.3826
3.5	0.4121	0.3993	0.3875	0.3847

Table 7. The local Sherwood Number $-\phi'(0)$ for different values of β and Kp

$Kp \downarrow \backslash \beta \rightarrow$	$-\phi'(0), \beta = 0.5$	$-\phi'(0), \beta = 1.0$	$-\phi'(0), \beta = 2.5$	$-\phi'(0), \beta = 3.5$
0.2	0.4934	0.4881	0.4836	0.4826
1.0	0.5049	0.5002	0.4961	0.4952
2.5	0.5075	0.5031	0.4992	0.4982
3.5	0.5081	0.5037	0.4998	0.4989

Table 8. The local Skin friction $f''(0)$ for different values of β and Fs

$Fs \downarrow \backslash \beta \rightarrow$	$\beta = 0.50$ local Skin friction ,	$\beta = 1.0$ local Skin friction ,	$\beta = 2.5$ local Skin friction ,	$\beta = 3.5$ local Skin friction ,
0.2	-0.7752	-0.9016	-1.0240	-1.0548
1.0	-0.8252	-0.9579	-1.0859	-1.1180
2.5	-0.9064	-1.0486	-1.1849	-1.2190
3.5	-0.9537	-1.1010	-1.2417	-1.2767

Table 9. The local Nusselt Number $-\theta'(0)$ for different values of β and Fs

$Fs \downarrow \backslash \beta \rightarrow$	$-\theta'(0), \beta = 0.5$	$-\theta'(0), \beta = 1.0$	$-\theta'(0), \beta = 2.5$	$-\theta'(0), \beta = 3.5$
0.2	0.4069	0.3929	0.3800	0.3769
1.0	0.4028	0.3885	0.3754	0.3723
2.5	0.3961	0.3813	0.3680	0.3649
3.5	0.3922	0.3772	0.3638	0.3607

Table 10. The local Sherwood Number $-\phi'(0)$ for different values of β and Fs

$Fs \downarrow \backslash \beta \rightarrow$	$-\phi'(0), \beta = 0.5$	$-\phi'(0), \beta = 1.0$	$-\phi'(0), \beta = 2.5$	$-\phi'(0), \beta = 3.5$
0.2	0.5065	0.5018	0.4977	0.4967
1.0	0.5049	0.5002	0.4961	0.4952
2.5	0.5025	0.4978	0.4937	0.4927
3.5	0.5011	0.4964	0.4923	0.4913

Table 11. The local Skin friction $f''(0)$ for different values of β and α

$\alpha \downarrow \backslash \beta \rightarrow$	$\beta = 0.50$ local Skin friction ,	$\beta = 1.0$ local Skin friction ,	$\beta = 2.5$ local Skin friction ,	$\beta = 3.5$ local Skin friction ,
0.2	-0.8252	-0.9579	-1.0859	-1.1180
1.0	-0.8564	-1.0001	-1.1398	-1.1751
2.5	-0.9580	-1.1419	-1.3291	-1.3779
3.5	-0.9689	-1.1580	-1.3528	-1.4047

Table 12. The local Nusselt Number $-\theta'(0)$ for different values of β and α

$\alpha \downarrow \backslash \beta \rightarrow$	$-\theta'(0), \beta = 0.5$	$-\theta'(0), \beta = 1.0$	$-\theta'(0), \beta = 2.5$	$-\theta'(0), \beta = 3.5$
0.2	0.4028	0.3885	0.3754	0.3723
1.0	0.3993	0.3830	0.3677	0.3640
2.5	0.3856	0.3590	0.3262	0.3159
3.5	0.3839	0.3554	0.3169	0.3029

Table 13. The local Sherwood Number $-\phi'(0)$ for different values of β and α

$\alpha \downarrow \backslash \beta \rightarrow$	$-\phi'(0), \beta = 0.5$	$-\phi'(0), \beta = 1.0$	$-\phi'(0), \beta = 2.0$	$-\phi'(0), \beta = 3.0$
0.2	0.5049	0.5002	0.4961	0.4952
1.0	0.5037	0.4986	0.4940	0.4930
2.5	0.4996	0.4926	0.4857	0.4840
3.5	0.4992	0.4919	0.4845	0.4825

Table 14. The local Skin friction $f''(0)$ for different values of β and n

$n \downarrow \backslash \beta \rightarrow$	$\beta = 0.50$ local Skin friction ,	$\beta = 1.0$ local Skin friction ,	$\beta = 2.5$ local Skin friction ,	$\beta = 3.5$ local Skin friction ,
0.5	-0.8673	-1.0079	-1.1437	-1.1778
1.0	-0.8252	-0.9579	-1.0859	-1.1180
2.0	-0.8111	-0.9393	-1.0622	-1.0930
3.0	-0.8331	-0.9625	-1.0863	-1.1172

Table 15. The local Nusselt Number $-\theta'(0)$ for different values of β and n

$n \downarrow \backslash \beta \rightarrow$	$-\theta'(0), \beta = 0.5$	$-\theta'(0), \beta = 1.0$	$-\theta'(0), \beta = 2.5$	$-\theta'(0), \beta = 3.5$
0.5	0.3970	0.3814	0.3672	0.3638
1.0	0.4028	0.3885	0.3754	0.3723
2.0	0.4066	0.3934	0.3815	0.3787
3.0	0.4061	0.3934	0.3821	0.3794

Table 16. The local Sherwood Number $-\phi'(0)$ for different values of β and n

$n \downarrow \backslash \beta \rightarrow$	$-\phi'(0), \beta = 0.5$	$-\phi'(0), \beta = 1.0$	$-\phi'(0), \beta = 2.5$	$-\phi'(0), \beta = 3.5$
0.5	0.5242	0.5202	0.5168	0.5160
1.0	0.5049	0.5002	0.4961	0.4952
2.0	0.4811	0.4753	0.4703	0.4691
3.0	0.4660	0.4594	0.4536	0.4523

Table 17. The local Skin friction $f''(0)$ for different values of β and Vs

$Vs \downarrow \backslash \beta \rightarrow$	$\beta = 0.50$ local Skin friction ,	$\beta = 1.0$ local Skin friction ,	$\beta = 2.5$ local Skin friction ,	$\beta = 3.5$ local Skin friction ,
0.2	-0.8252	-0.9579	-1.0859	-1.1180
1.0	-0.4525	-0.4884	-0.5184	-0.5254
2.5	-0.2490	-0.2584	-0.2656	-0.2672
3.5	-0.1920	-0.1971	-0.2008	-0.2016

Table 18. The local Nusselt Number $-\theta'(0)$ for different values of β and Vs

$Vs \downarrow \backslash \beta \rightarrow$	$-\theta'(0), \beta = 0.5$	$-\theta'(0), \beta = 1.0$	$-\theta'(0), \beta = 2.5$	$-\theta'(0), \beta = 3.5$
0.2	0.4028	0.3885	0.3754	0.3723
1.0	0.3633	0.3494	0.3383	0.3358
2.5	0.3343	0.3245	0.3173	0.3158
3.5	0.3249	0.3170	0.3114	0.3103

Table 19. The local Sherwood Number $-\phi'(0)$ for different values of β and Vs

$Vs \downarrow \backslash \beta \rightarrow$	$-\phi'(0), \beta = 0.5$	$-\phi'(0), \beta = 1.0$	$-\phi'(0), \beta = 2.5$	$-\phi'(0), \beta = 3.5$
0.2	0.5049	0.5002	0.4961	0.4952
1.0	0.4891	0.4851	0.4820	0.4813
2.5	0.4790	0.4765	0.4747	0.4744
3.5	0.4759	0.4741	0.4728	0.4725

From Table 3 we observe that considering the value of the magnetic parameter $\boldsymbol{M}$ as fix, we observe that, with the increase in the value of Casson parameter β, local skin friction $f''(0)$ decreases and considering the value of Casson parameter β as fix we observe that with the increase in the value of the magnetic parameter, $\boldsymbol{M}$, local skin friction $f''(0)$ decreases.

From Table 4 we observe that considering the value of the magnetic parameter $\boldsymbol{M}$, as fix ,we observe that, with the increase in the value of the Casson parameter β , Local Nusselt Number $-\theta'(0)$ decreases and considering the value of Casson parameter β as fix we observe that with the increase in the value of the magnetic parameter, $\boldsymbol{M}$, Local Nusselt Number $-\theta'(0)$ decreases.

From Table 5 we observe that considering the value of the magnetic parameter $\boldsymbol{M}$, as fix ,we observe that, with the increase in the value of the Casson parameter β , Local Sherwood Number $-\phi'(0)$ decreases and considering the value of Casson parameter β as fix we observe that with the increase in the value of the magnetic parameter, $\boldsymbol{M}$, Local Sherwood Number $-\phi'(0)$ decreases.

From Table 6 we observe that considering the value of the porosity parameter $\boldsymbol{Kp}$ as fix, we observe that, with the increase in the value of Casson parameter β, local skin friction $f''(0)$ decreases and considering the value of Casson parameter β as fix we observe that with the increase in the value of the porosity parameter $\boldsymbol{Kp}$, local skin friction $f''(0)$ increases.

From Table 7 we observe that considering the value of the porosity parameter $\boldsymbol{Kp}$, as fix ,we observe that, with the increase in the value of the Casson parameter β, Local Nusselt Number $-\theta'(0)$ decreases and considering the value of Casson parameter β as fix we observe that with the increase in the value of the porosity parameter $\boldsymbol{Kp}$, Local Nusselt Number $-\theta'(0)$ increases.

From Table 8 we observe that considering the value of the porosity parameter $\boldsymbol{Kp}$, as fix ,we observe that, with the increase in the value of the Casson parameter β, Local Sherwood Number $-\phi'(0)$ decreases and considering the value of Casson parameter β as fix we observe that with the increase in the value of the porosity parameter $\boldsymbol{Kp}$, Local Sherwood Number $-\phi'(0)$ increases.

From Table 9 we observe that considering the value of the Forchheimer parameter $\boldsymbol{Fs}$ as fix, we observe that, with the increase in the value of Casson parameter β, local skin friction $f''(0)$ decreases and

considering the value of Casson parameter β as fix we observe that with the increase in the value of the Forchheimer parameter $\boldsymbol{Fs}$, local skin friction $f''(0)$ decreases.

From Table 10 we observe that considering the value of the Forchheimer parameter $\boldsymbol{Fs}$, as fix ,we observe that, with the increase in the value of the Casson parameter β , Local Nusselt Number $-\boldsymbol{\theta'(0)}$ decreases and considering the value of Casson parameter β as fix we observe that with the increase in the value of the Forchheimer parameter $\boldsymbol{Fs}$, Local Nusselt Number $-\boldsymbol{\theta'(0)}$ decreases.

From Table 11 we observe that considering the value of the Forchheimer parameter $\boldsymbol{Fs}$, as fix ,we observe that, with the increase in the value of the Casson parameter β , Local Sherwood Number $-\boldsymbol{\phi'(0)}$ decreases and considering the value of Casson parameter β as fix we observe that with the increase in the value of the Forchheimer parameter $\boldsymbol{Fs}$, Local Sherwood Number $-\boldsymbol{\phi'(0)}$ decreases.

From Table 12 we observe that considering the value of the inclination parameter $\boldsymbol{\alpha}$, as fix ,we observe that, with the increase in the value of Casson parameter β , local skin friction $\boldsymbol{f''(0)}$ decreases and considering the value of Casson parameter β as fix we observe that with the increase in the value of the inclination parameter $\boldsymbol{\alpha}$, local skin friction $f''(0)$ decreases.

From Table 13 we observe that considering the value of the inclination parameter $\boldsymbol{\alpha}$, as fix ,we observe that, with the increase in the value of the Casson parameter β, Local Nusselt Number $-\boldsymbol{\theta'(0)}$ decreases and considering the value of Casson parameter β as fix we observe that with the increase in the value of the inclination parameter $\boldsymbol{\alpha}$, Local Nusselt Number $-\boldsymbol{\theta'(0)}$ decreases.

From Table 14 we observe that considering the value of the inclination parameter $\boldsymbol{\alpha}$, as fix ,we observe that, with the increase in the value of the Casson parameter β, Local Sherwood Number $-\boldsymbol{\phi'(0)}$ decreases and considering the value of Casson parameter β as fix we observe that with the increase in the value of the inclination parameter $\boldsymbol{\alpha}$, Local Sherwood Number $-\boldsymbol{\phi'(0)}$ decreases.

From Table 15 we observe that considering the value of the stretching index parameter $\boldsymbol{n}$, as fix ,we observe that, with the increase in the value of Casson parameter β, local skin friction $\boldsymbol{f''(0)}$ decreases and considering the value of Casson parameter β as fix we observe that with the increase in the value of the stretching index parameter $\boldsymbol{n}$, local skin friction $f''(0)$ increases.

From Table 16 we observe that considering the value of the stretching index parameter $\boldsymbol{n}$, as fix ,we observe that, with the increase in the value of the Casson parameter β , Local Nusselt Number $-\boldsymbol{\theta'(0)}$ decreases and considering the value of Casson parameter β as fix we observe that with the increase in the value of the stretching index parameter $\boldsymbol{n}$, Local Nusselt Number $-\boldsymbol{\theta'(0)}$ increases.

From Table 17 we observe that considering the value of the stretching index parameter n, as fix, we observe that, with the increase in the value of the Casson parameter β, Local Sherwood Number $-\boldsymbol{\phi'(0)}$ decreases and considering the value of Casson parameter β as fix we observe that with the increase in the value of the stretching index parameter n, Local Sherwood Number $-\boldsymbol{\phi'(0)}$ decreases.

From Table 18 we observe that considering the value of the velocity slip parameter Vs, as fix ,we observe that, with the increase in the value of Casson parameter β, local skin friction $\boldsymbol{f''(0)}$ decreases and considering the value of Casson parameter β as fix we observe that with the increase in the value of the velocity slip parameter Vs, local skin friction $f''(0)$ increases.

From Table 19 we observe that considering the value of the velocity slip parameter Vs, as fix ,we observe that, with the increase in the value of the Casson parameter β , Local Nusselt Number $-\boldsymbol{\theta'(0)}$ decreases and considering the value of Casson parameter β as fix we observe that with the increase in the value of the velocity slip parameter Vs, Local Nusselt Number $-\boldsymbol{\theta'(0)}$ decreases.

From Table 20 we observe that considering the value of the velocity slip parameter Vs, as fix ,we observe that, with the increase in the value of the Casson parameter β , Local Sherwood Number $-\boldsymbol{\phi'(0)}$ decreases

and considering the value of Casson parameter β as fix we observe that with the increase in the value of the velocity slip parameter Vs, Local Sherwood Number $-\boldsymbol{\phi}'(\mathbf{0})$ decreases.

5 Conclusion

In this paper we have studied numerical analysis of the flow of Casson fluid under the influence of magnetic field applied in the transverse direction to the flow of the fluid and fluid flows through the non-Darcy porous medium, with velocity slip, the surface over which fluid flows, is non linear and inclined at some angle to the vertical. And the flow of the fluid is due to the stretching of the surface. In the mathematical model, we have transformed the momentum equation, energy equation and mass concentration equations to non-dimensional ordinary differential equations using similarity variables. We have solved the equations numerically by bvp4c using MATLAB for the numerical computation, and took $\eta_\infty = 12$, and axes so that figures are clearly visible. We have discussed and analysed the magnitude of the velocity, temperature, concentration, Local Skin friction, Local Nusselt number and Local Sherwood number using their representative parameters and the effects of these parameters on the respective boundary layer regions using graphs, figures and tables.

Above results and discussion give us the following conclusions:

Figures show following conclusions:

(i) With the increase in the value of magnetic, Forchheimer, inclination parameter, or Casson, the velocity boundary layer thickness and the absolute value of velocity decrease.

(ii) With the increase in the value of magnetic, Forchheimer, inclination parameter, Casson , or velocity slip parameter the thermal boundary layer thickness and the absolute value of temperature increase.

(iii) With the increase in the value of magnetic, Forchheimer, inclination, Casson , stretching index or velocity slip parameter, the concentration boundary layer thickness and the absolute value of concentration increase.

(iv) With the increase in the value of porosity, or stretching index parameter, the velocity boundary layer thickness and the absolute value of velocity increase.

(v) With the increase in the value of porosity, or stretching index parameter, thermal boundary layer thickness and the absolute value of temperature decrease.

(vi) With the increase in the value of porosity parameter, the concentration boundary layer thickness and the absolute value of concentration decrease.

(vii) With the increase in the value of velocity slip parameter near the left of similarity variable having value 3, the velocity boundary layer thickness and the absolute value of velocity decrease and this variation slows down with the increase in the value of velocity slip parameter, while near to the right of similarity variable having value 3, the velocity boundary layer thickness and the absolute value of velocity begins to increase and this variation speeds up with the increase in the value of velocity slip parameter.

Tables show following conclusion:

(viii) With the increase in the value of Casson parameter considering magnetic, porosity, Forchheimer, inclination, stretching index or velocity slip parameter fix, we observe that the local skin friction, local Nusselt number or local Sherwood number decreases.

(ix) With the increase in the value of porosity parameter considering Casson parameter fix we observe that local skin friction local Nusselt Number or local Sherwood Number increases.

(x) With the increase in the value of stretching index parameter considering Casson parameter fix we observe that local skin friction or local Nusselt Number increases but local Sherwood number decreases.

(xi) With the increase in the value of velocity slip parameter considering Casson parameter fix we observe that local skin friction increases but local Nusselt Number or local Sherwood Number decreases.

Acknowledgement

Author thanks to the Department of Mathematics, SOPS, Doon University, Dehradun, India, for its help in the work.

Competing Interests

Authors have declared that no competing interests exist.

References

[1] Lawrence J. Crane. Flow past a stretching plate. Kurze Mitteilungen, Brief Report- Communications Breves. 1970;21.

[2] Rajagopal KR, Na TY, Gupta AS. Flow of viscoelastic fluid over a stretching sheet. Rheologica Acta. 1984;23:213-215.

[3] Ishak Anuar, Nazar Roslinda, Pop Ioan. Falkner-Skan equation for flow past a moving wedge with suction or injection. J. Appl. Math. & Computing. 2007;25(1-2):67-83.
Available:http://jamc.net

[4] Siddappa B, Abel Subhas. Non-Newtonian flow past a stretching plate. Journal of Applied Mathematics and Physics (ZAMP). 1985;36.

[5] Andersson HL. Note: MHD flow of a viscoelastic fluid past a stretching surface. Acta Mechanica. 1992;95:227-230.

[6] Dandapat BS, Holmedal LE, Andersson HL. Note: On the stability of MHD flow of a viscoelastic fluid past a stretching sheet. Acta Mechanica. 1998;130:143-146.

[7] Fang Tiegang, Guo Fang, Lee Chia-Fon F. A note on the extended Blasius equation. Applied Mathematics Letters. 2006;19:613–617.
Available:www.sciencedirect.com

[8] Mamaloukas Ch, Spartalis S, Manussaridis Z. Similarity approach to the problem of second grade fluid flows over a stretching sheet. Applied Mathematical Sciences. 2007;1(7):327–338.

[9] Khidir Ahmed. A note on the solution of general Falkner-Skan problem by two novel semi-analytical techniques. Propulsion and Power Research. 2015;4(4):212–220.
Available:http://ppr.buaa.edu.cn/,www.sciencedirect.com

[10] Bataller Rafael Cortell. Numerical comparisons of Blasius and Sakiadis flows. Matematika. 2010;26(2):187-196.

[11] Motsa SS, Hayat T, Aldossary OM. MHD flow of upper-convected Maxwell fluid over porous stretching sheet using successive Taylor series linearization method. Appl. Math. Mech. -Engl. Ed. 2012;33(8):975–990.
DOI: 10.1007/s10483-012-1599-x

[12] Motsa Sandile Sydney, Sibanda Precious. On the solution of MHD flow over a nonlinear stretching sheet by an efficient semi-analytical technique. International Journal for Numerical Methods in Fluids; 2012.
DOI: 10.1002/fld.2541

[13] Rosca A. MHD boundary-layer flow over a permeable shrinking surface. Acta Universitatis Apulensis. 2013;36:31-38. ISSN: 1582-5329.

[14] Nadeem S, Hussain ST, Lee Changhoon. Flow of a Williamson fluid over a stretching sheet. Brazilian Journal of Chemical Engineering. 2013;30(03):619–625.

[15] Mukhopadhyay Swati. MHD boundary layer slip flow along a stretching cylinder. Ain Shams Engineering Journal. 2013;4:317–324.
Available:www.sciencedirect.com

[16] Akbar NS, Nadeem S, Haq Rizwan Ul, Ye Shiwei. MHD stagnation point flow of Carreau fluid toward a permeable shrinking sheet: Dual solutions. Ain Shams Engineering Journal. 2014;5:1233–1239.
Available:www .elsevier .com /locate /asej, www.sciencedirect.com

[17] Nadeem S, Haq Rizwan Ul, Lee C. Research note: MHD flow of a Casson fluid over an exponentially shrinking sheet. Scientia Iranica B. 2012;19(6):1550–1553.
Available:www.sciencedirect.com

[18] Biswas R, Mondal M, Sarkar DR, Ahmmed SF. Effects of radiation and chemical reaction on MHD unsteady heat and mass transfer of Casson fluid flow past a vertical plate. Journal of Advances in Mathematics and Computer Science. 2017;23(2):1-16.
Available:http://www.science domain.org/issue/2795

[19] Ahmmed SF, Biswas R, Afikuzzaman M. Unsteady MHD free convection flow of nanofluid through an exponentially accelerated inclined plate embedded in a porous medium with variable thermal conductivity in the presence of radiation. Journal of Nanofluids. 2018;7:891-901.
Available:http://www.aspbs. com/jon.htm.

[20] Biswas Rajib, Ahmmed Sarder Firoz. Effects of Hall current and chemical reaction on MHD unsteady heat and mass transfer of Casson nanofluid flow through a vertical plate. Journal of Heat Transfer.
Available:http://asmedigital collection.asme.org

[21] Noor Khan Saeed, Zuhra Samina, Shah Zahir, Bonyah Ebenezer, Khan Waris, Saeed Islam, Khan Aurangzeb. Hall current and thermophoresis effects on magnetohydrodynamic mixed convective heat and mass transfer thin film flow. Journal of Physics Communications; 2018.
Available:https://doi.org/10.1088/2399-6528/aaf830

[22] Sharada K, Shankar B. MHD mixed convection flow of a Casson fluid over an exponentially stretching surface with the effects of soret, dufour, thermal radiation and chemical reaction. World Journal of Mechanics. 2015;5:165-177.
Available:http://dx.doi.org/10.4236/wjm.2015.59017

[23] Mukhopadhyay Swati, Krishnendu Bhattacharyya, Tasawar Hayat. Exact solutions for the flow of Casson fluid over a stretching surface with transpiration and heat transfer effects. Chin. Phys. 2013;22(11):114701.
DOI: 10.1088/1674-1056/22/11/114701

[24] Raza Jawad, Fateh Mebarek-Oudina, Mahanthesh B. Magnetohydrodynamic flow of nano Williamson fluid generated by stretching plate with multiple slips. Multidiscipline Modeling in Materials and Structures. 2019;15(5):871-894. © Emerald Publishing Limited. 1573-6105.
DOI: 10.1108/MMMS-11-2018-0183

[25] Raza Jawad, Mushayydha Farooq, Fateh Mebarek-Oudina, Mahanthesh B. Multiple slip effects on MHD non-Newtonian nanofluid flow over a nonlinear permeable elongated sheet numerical and statistical analysis. Multidiscipline Modeling in Materials and Structures. 2019;15(5):913-931. © www.emeraldinsight.com/1573-6105.htm.
DOI: 10.1108/MMMS-11-2018-0190.

[26] Mebarek -Oudina F. Convective heat transfer of Titania nanofluids of different base fluids in cylindrical annulus with discrete heat source. Heat Transfer—Asian Res. 2018;1-13. © 2018 wileyonlinelibrary.com/journal/htj.
DOI: 10.1002/htj.21375

[27] Mahanthesh Basavarajappa, Giulio Lorenzini, Feteh Mebarek Oudina, Isac Lare Animasaun. Significance of exponential space- and thermal-dependent heat source effects on nanofluid flow due to radially elongated disk with Coriolis and Lorentz forces. Journal of Thermal Analysis and Calorimetry.
Available:https://doi.org/10.1007/s10973-019-08985-0

[28] Marzougui S, Fateh Mebarek-Oudina, Assia A, Magherbi M, Zahir Shah, Ramesh K. Entropy generation on magneto-convective flow of copper–water nanofluid in a cavity with chamfers. Journal of Thermal Analysis and Calorimetry.
Available:https://doi.org/10.1007/s10973-020-09662-3

[29] Raza J, Mebarek-Oudina F, Ram P, Sharma S. MHD flow of non-Newtonian molybdenum disulfide nanofluid in a converging/diverging channel with Rosseland radiation. Defect and Diffusion Forum Submitted. 2019;401:92-106. ISSN: 1662-9507, © 2020 Trans Tech Publications Ltd, Switzerland.

[30] Kala Bhim Sen. The numerical analysis of the effect of Grashof number, modified Grashof number and chemical reaction on the non-Darcy MHD flow of a Casson fluid over a nonlinearly stretching sheet in a porous medium. International Journal of Scientific Research in Physics and Applied Sciences. 2019;7(3):49-70. E-ISSN: 2348-3423.
DOI: https://doi.org/10.26438/ijsrpas/v7i3.4970

[31] Kala Bhim Sen. The numerical analysis of the effect of suction, slip and inclination, on the non-Darcy MHD flow of a Casson fluid over a nonlinearly stretching sheet in a porous medium. International Journal of Scientific Research in Mathematical and Statistical Sciences. 2019;6(3):55-78. E-ISSN: 2348-4519.
DOI: https://doi.org/10.26438/ijsrmss/v6i3.5578

[32] Kala Bhim Sen. Analysis of non-Darcy MHD flow of a Casson fluid over a non-linearly stretching sheet with partial slip in a porous medium. AJARR. 2019;3(3):1-15.

Peer-review history:
The peer review history for this paper can be accessed here (Please copy paste the total link in your browser address bar)
http://www.sdiarticle4.com/review-history/56956